Experiment on tuned open-test-case fan ECL5/CATANA: Structural characterization under vacuum conditions

K Billon, L Sanchez, G Bouvard, C Gibert, L Blanc, F Thouverez

▶ **To cite this version:**

K Billon, L Sanchez, G Bouvard, C Gibert, L Blanc, et al.. Experiment on tuned open-test-case fan ECL5/CATANA: Structural characterization under vacuum conditions. TurboExpo 2024, ASME, Jun 2024, Londres, United Kingdom. hal-04679347

HAL Id: hal-04679347
https://hal.science/hal-04679347v1

Submitted on 28 Aug 2024

HAL is a multi-disciplinary open access archive for the deposit and dissemination of scientific research documents, whether they are published or not. The documents may come from teaching and research institutions in France or abroad, or from public or private research centers.

L'archive ouverte pluridisciplinaire **HAL**, est destinée au dépôt et à la diffusion de documents scientifiques de niveau recherche, publiés ou non, émanant des établissements d'enseignement et de recherche français ou étrangers, des laboratoires publics ou privés.

Experiment on tuned open-test-case fan ECL5/CATANA: Structural characterization under vacuum conditions

K. Billon[a], L. Sanchez[a], G. Bouvard[a], C. Gibert[a], L. Blanc[a], and F. Thouverez[a]

[a]Ecole Centrale de Lyon, CNRS, ENTPE, LTDS, UMR5513, 69130 Ecully, France

ABSTRACT

The CATANA project aims to promote the development of the next generation of Ultra-High-Bypass-Ratio Turbofan engines by closing the knowledge gaps concerning multi-physical interactions which affect performance and limit the stability range. It involves a composite-material fan stage, called ECL5, representative of near future UHBR architectures. It has been designed at Ecole Centrale de Lyon to provide an open for the community benchmark configuration. This fan had been extensively tested previously at the aerodynamic Phare-2 test facility (rotating machinery platform for environmental risk control) in different running conditions at the LMFA laboratory (Ecole Centrale de Lyon fluid mechanics and acoustics laboratory) concerning synchronous and asynchronous responses (NSV).

It is tested here under vacuum, in rotating conditions in the Phare-1 facility in order to identify structural modal parameters, ie mainly the whole fan blade assembly structural damping. Each blade is equipped with piezoelectric actuators to excite structural modes. Blades' vibratory responses are measured via embedded strain gauges. The instrumented fan blades are firstly individually tested on a specific test hub mounting. Piezoelectric actuators efficiency is demonstrated by reaching representative amplitudes. Also, individual blades frequencies dispersion is quantified and shows in particular that the added exciters have negligible influence on mistuning and dynamics. The fan response is measured using the same instrumentation as for aerodynamic experiments and at the same rotational speed. Influence of rotating speed and vibration level on modal damping is shown and quantified.

Nomenclature

Acronyms

— 1F : First bending mode
— 2F : Second bending mode
— CFD : Computational Fluid Dynamics
— FEM : Finite Element Method
— Phare−1 : Vacuum structural test rig
— Phare−2 : Aerodynamic test rig
— FRF : Frequency response function
— LCO : Limit Cycle of Oscillations
— ND : Nodal Diameter
— NSV : Non-Synchronous Vibration
— PZT : Lead zirconate titanate piezoelectric material
— SDOF : Single Degree Of Freedom
— SV : Synchronous Vibration
— LSRF : Least squares rational function method
— TW : Travelling wave
— UHBR : Ultra-High-Bypass-Ratio

Further author information: (Send correspondence to Kevin Billon)
E-mail: kevin.billon@ec-lyon.fr

Notations

— f : Frequency $[Hz]$
— k : Blade index number in fan assembly $[-]$
— N : Number of blades $[-]$
— Nn : Maximum rotor speed percentage [%]
— N_ν : Nodal diameter index number $[-]$
— t : Time $[s]$
— $U(t)$: TW excitation vector, $N \times 1$, components $U_k(t)$ $[V]$
— U_f : Forward part amplitude of $U(t)$, real $[V]$
— U_b : Backward part amplitude of $U(t)$, real $[V]$
— ε : Strain $[\mu def]$ or alternatively $[\mu m/m]$
— ξ : Viscous damping ratio [%]
— ω : Angular frequency $[rad/s]$
— Ω : Rotor speed $[rpm]$

Introduction

Fans aeroelastic stability has been a major point of interest in turbomachinery design for decades and becomes more and more critical in a context of fuel consumption reduction objectives. Indeed engine manufacturers need to reduce dry masses without impairing life expectancy or engine global performance. For the family of designs addressed here, high performance composite material blades are used.[1] Such technologies enable larger turbojet engine building by maximizing the bypass flow on future Ultra-High-Bypass-Ratio turbofan engines. But they lead to highly-coupled fluid-mechanical instability mechanisms inducing operating limits for which long established design criteria need revisiting. Destabilizing conditions can arise from aerodynamic, aeroelastic and aeroacoustic phenomena such as flutter, non-synchronous blade vibrations (NSV) or rotating stall : all can occur in experimental conditions at subsonic or transonic speeds.[2] But stability limits do not only depend on the excitation and damping brought by the flow, they also depend on the purely structural damping brought by blade material and joints between blades and hub disk. In stable functioning conditions too, blade vibration amplitude, and then material fatigue and blades life expectancy directly depend on structural properties.

Technically, composite blades are assembled to the hub through dovetail attachments (Figures 2, 3). Such attachment systems are also present on compressor or turbine designs. Non-linear friction occurs, entailing several effects. Firstly, energy dissipation occurs, contributing to vibration level mitigation because energy provided to the structure by the flow is changed in heat by friction. Secondly, system's free dynamics is also changed, as well in terms of free frequency of vibrations or mode shapes. Typically, focusing for example on the flutter phenomenon, it has been shown that non-linear structural phenomena can reduce flutter impact by saturating blades vibration amplitude : limit cycle of oscillations (LCOs) occur beyond the stability limits predicted by linear structure models. Several numerical studies focus on predicting such LCOs on industrial structures : using non-linear complex modes to quantify single mode flutter amplitudes on a fan,[3] or using direct time-integration quantify flutter and forced response vibrations interaction on a compressor.[4] Such models or[5] require experiments for the sake of comparison.

The present study is based on the CATANA project ECL5 open test-case configuration.[1] The global objective is to analyse and interpret highly-coupled fluid-mechanical instability mechanisms from a representative composite UHBR fan to enable more accurate prediction methods. The envisaged concept here is to provide detailed structural analysis and to perform exhaustive steady and transient investigations with synchronized multi-physical instrumentation at all critical limits of the operating range. In CATANA, two categories of tests are performed. The first category includes fully coupled tests, involving fluid mechanics as well as structural phenomena, they are performed in Phare-2 fluid vein in rotating conditions.[2] The second category focuses on structural phenomena : they are performed on Phare-1 facility without the fluid, in vacuum, and in rotating conditions.

The great benefit, apart from the open-to-the-community configuration, is the complementarity, on a same test case of such experiments. Indeed, the originality of the study lies in the fact that it is the first time to author's

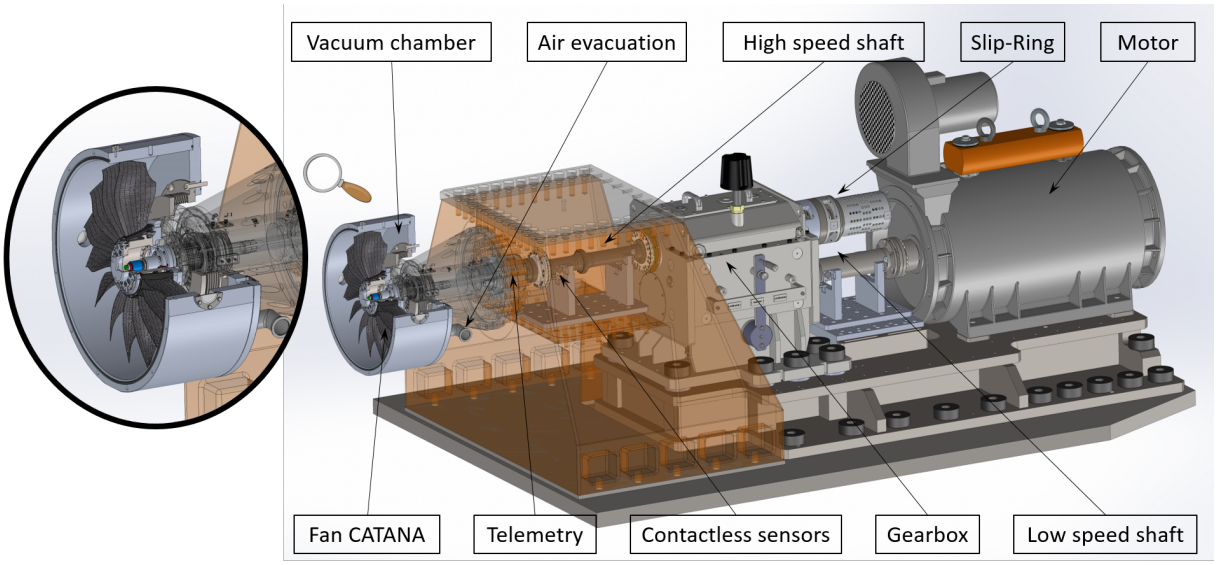

FIGURE 1. General view of the Phare-1 vacuum test rig facility at LTDS.

knowledge, that a same composite fan specimen has been tested in aerodynamic conditions and then at vacuum at equivalent conditions in term of speed and vibration state. Indeed, Phare-1 test rig is dedicated to experimental studies on full scale rotating industrial fans or compressor bladed disks at their operating conditions and focusing on the structural dynamics behaviour. Basically the fluid-structure coupling interaction is suppressed as the experiments are performed in vacuum. Also, these conditions allow to drive the specimen using a relatively small amount of power. While aeroelastic excitations are removed, a very versatile piezoelectric excitation system is used for generating vibrations needed for modal testing. The influence on blade response of experiment parameters – namely rotating speed, excitation spectrum, excitation strength and spatial distribution over the fan or compressor - can then be accurately investigated.

Concerning mechanics, here, the strategy is to concentrate on without-the-flow characterisation to split the global modelling difficulty by enabling non-linear mechanical model updating in terms of modal properties - depending on rotational speed, friction contact conditions and vibration amplitude.[6] The benefits of performing tests in vacuum, when blade – disk contact needs centrifugation to be effective, is not only at the level of structural "purity" - this last term meaning that air damping is removed from the total damping measured in the modal characterization. But conversely, total damping measured in the flow will potentially be diminished from structural damping to better fit aerodynamic damping predicted from purely CFD computations. At the end (not in this paper), further developments will rely on the data obtained here in "simpler" conditions to feed models fitting Phare-2 with-the-fluid experiments in a context of increased fluid-structure description fidelity.

The first section presents the tuned configuration test case and the instrumentation used for its comprehensive investigation under vacuum. The experimental means of performing the rotational tests, conditions and methods used to estimate the modal parameters from the measured frequency response data are presented in the second section. The final section presents the results in terms of modal parameters together with their sensitivity to the speed and excitation amplitude.

1. FAN AND INSTRUMENTATION DESCRIPTION

1.1 Tuned fan open test case

A new 1 :3 reduced scale fan stage, called ECL5 (diameter 500 mm), representative of near future UHBR fan concepts has been designed at Ecole Centrale de Lyon and manufactured from pre-impregnated carbon fiber layers. The geometry has been shared with the community as an open test case.[1] A subset of 16 blades has been selected among 48 ones produced, based on a minimum dispersion criterion on individual blade

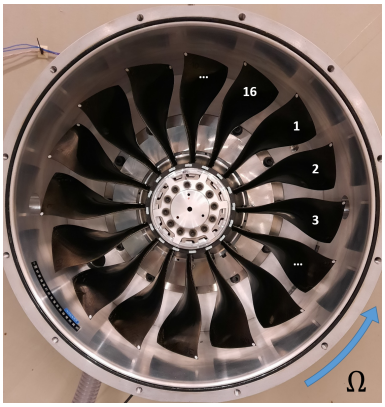

FIGURE 2. ECL 5 composite fan blade stage installed in Phare−1 test rig under vacuum conditions (rotating speed Ω, blade/slot numbers in white), the numbering convention is taken into account for generating forward/backward travelling waves with regard to rotating speed direction.

frequencies, to make a so-called reference tuned configuration. Recently, the first aerodynamic experiments have been performed on the Phare-2 test facility.[7]

The present paper discusses tests performed under vacuum condition on the Phare-1 test rig for this tuned fan structural characterisation purposes. The investigated specimen consists of the tuned configuration blade set, mounted on a titanium disk together with inter-blade platforms (Figure 2). Disk's geometry and material are, locally to blades, similar to Phare-2's arrangement to ensure the best possible mechanical system representativeness. Original disk's rear part design has only been adapted to match Phare-1 mechanical interfaces (see zoomed-in view in Figure 1 and FEM model of Phare-2 disc in Figure 3).

Furthermore, blades and inter-blade platforms' positions on the disk, identified by their serial number, are exactly reproduced from[2] experiments. A difference could be caused by the additional piezoelectric actuators used for modal tests, which could not be installed before aerodynamic tests, due Phare-1 and Phare-2 experiments respective schedules. This is discussed in detail below.

1.2 Piezoelectric excitation system

Since fluid-structure coupling interaction is suppressed in vacuum, a piezoelectric system is used to generate the forces required for vibration testing. It has to be positioned in order to satisfy given objectives in terms of representative amplitudes (a percent of the scope limit) of Phare-2 experiments[2] for given modes of interest (first and second bending modes). This part describes the process for piezoelectric instrumentation positioning on the blade, using numerical and experimental approaches.

1.2.1 Actuators optimal positioning

FEM model description. The first step is to find piezoelectric actuators optimal positioning using an electromechanical finite element model. Initial mechanical model (Figure 3) was developed by LMFA through commercial finite element software composite module.[1] Here, due vacuum conditions, air pressure on blades is removed. Cyclic symmetry conditions are applied on single sector mesh boundaries. Note that this physically implies an assumption on blade set perfect tuning. 0ND modes phase conditions are used for correlation with single blade tests described below whereas $N_\nu > 0$ modes are used to predict rotating tests in a further step. Composite blades have orthotropic material properties, homogenised by classical laminate theory. Blade and disk meshes are coincident at dovetail attachment interface : a perfect node-to-node connection is assumed. Disk is meshed using 15885 tetrahedral structural 10-nodes elements. Blade's mesh contains 8959 hexahedral structural 20-nodes elements and piezoelectric elements use 64 hexahedral coupled field piezoelectric 20-nodes elements. Blade and actuator meshes are also coincident and structural degrees of freedom are node-to-node coupled. Note that platforms are not included at this step, for simplicity reasons, therefore it is assumed that they do not have any major impact on piezoelectric actuator design.

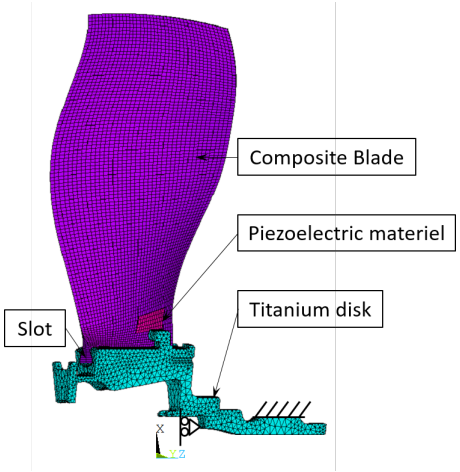

FIGURE 3. ECL5 bladed disk assembly's single sector electro-mechanical FEM mesh (CATANA Blade ECL5v5).

Piezoelectric material modelling. Actuators material piezoelectric properties are taken from the technical documentation of a commercially available lead zirconate titanate (PZT) encapsulated patch actuator. The poling axis of the piezoelectric material is defined orthogonal to the surface where the actuator is placed on the blade. The main parameter influencing the force transmitted from the actuator to the structure is the piezoelectric charge constant $d_{31} = -180 \times 10^{-12}\ C/N$. The encapsulation of the PZT material is not taken into account at this stage as it is not documented by the manufacturer. For the calculation process, a first non-linear static pre-stress calculation under centrifugal loading (from 0 to 100% Nn) is performed. A pre-stressed modal analysis is performed, followed by a fully pre-stressed harmonic response to obtain the frequency response to a voltage excitation of amplitude 200 V (maximum design value). A proportional damping model is assumed, corresponding to a pre-supposed modal damping ratio (ξ) equal to 0.2% for the harmonic response. Frequency response displacements are calculated at the blade tip leading edge along the engine axis (Z).

Optimal location scanning strategy. Harmonic response's amplitude depends on piezoelectric actuators' position. Basically, efficiency, along with K coefficient, is high when actuator is close to high elastic strain area. Constraints on positioning are as follows : strain gauges are already present, moreover actuators must be placed under platforms, indeed, no piezoelectric patch is tolerated on air-foils for future reuse in aerodynamic tests. Then, pressure and suction side areas are scanned independently of size 5 mm by 5 mm elementary piezoelectric patches to produce efficiency maps (Figures 5). For each elementary patch, resulting displacement's maximum amplitude is given at its location. Figures 4 and 5 illustrate parametric study results on pressure side. Piezoelectric patchs' centers are located by red circles (13×4 grid) with $[x, z]$ coordinates in Figure 4 (or alternatively by $[x_{ind}, z_{ind}]$ indices in Figure 5. Purple circles represent strain gauge locations, on which actuators cannot be placed.

Finally, most efficient areas are evaluated on both pressure and suction sides for both 1F and 2F bending modes. Commercially available piezoelectric patches, with piezoelectric material dimensions $20 \times 10 \times 0.5\ mm^3$, were selected and their positions adjusted to both sides of the blade. This actuator's geometry is represented by the black rectangle in Figures 5a and 5b. at its optimum position for both modes 1F and 2F labelled "zone 1g" for the pressure side.

1.2.2 Blades' instrumentation implementation

Each blade delivered for structural testing was already instrumented with a strain gauge on the suction side, which was used during Phare-2 aerodynamic tests, and some blades were instrumented with a second strain gauge on the pressure side. Suction side gauges were reused, allowing direct comparison between vacuum and aerodynamic tests responses. Pressure side strain gauges had to be removed to make room for the piezoelectric installation.

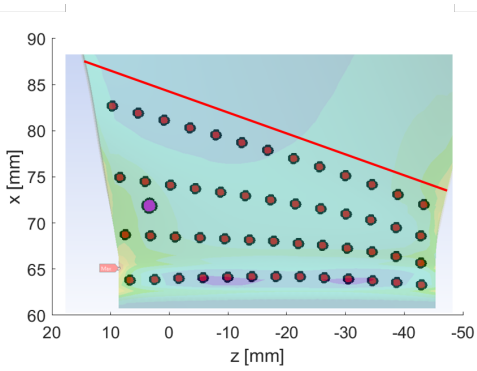

FIGURE 4. Spatial distribution of elementary piezoelectric patches center positions used for building efficiency maps. The von Mises modal strain distribution for the 1F mode is superimposed - Pressure side. Red line stands for inter-blade platform location.

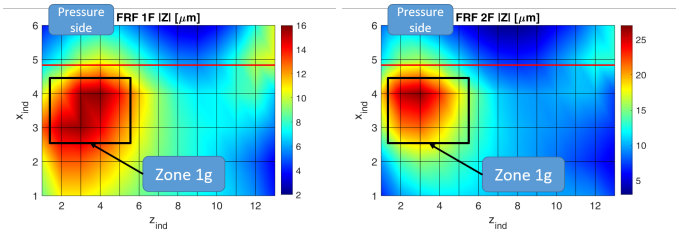

(a) (b)

FIGURE 5. Actuators efficiency maps - Frequency response amplitudes at resonance for each elementary actuator for the two modes of interest. Red line : free area limit under inter-blade platform. Black rectangle : actual piezoelectric material area (20 $mm \times 10\ mm$). a) 1F, b) 2F.

Blades are additionally instrumented with commercially available piezoelectric actuators, glued at locations defined above. The entire 16-blades set is deal with in a controlled manner, using a heated vacuum bag to ensure process uniformity, both in temperature and applied pressure useful to conform actuators to blades' curved surfaces. Actuator's position, adhesive quantity and temperature curing schedule are carefully controlled.

All instruments' correct and homogeneous functioning is checked on individual blades, clamped on the fixing hub, after piezoelectric patch installation, as described below.

1.2.3 Single blade electro-mechanical assessment

Objectives. This part is dedicated, first, to piezoelectric actuators performance experimental verification, with respect to the targeted strain amplitude levels : on the order of 200 μdef for SV, 100 μdef for NSV (respectively 20 μdef for SV, 100 μdef for NSV) for the first (respectively second) bending mode. These levels are primary objectives derived from.[2] Actuators non-intrusiveness and effectiveness homogeneity is also verified. Blades set's mistuning should not be affected by these new devices in order vacuum measurements to remain comparable with aerodynamic ones. The quality of the excitation used for the whole fan, as described below, is then verified by quantifying discrepancies between each blade's electromechanical properties.

Secondly, the single blade electromechanical model is updated, at rest on the fixing hub, so that this study can be extended next to the cyclic symmetry model under rotation. The purpose is to predict with confidence the whole fan dynamics, including rotational speed (Ω) influence. These effects are not detailed here, but the efficiency of the actuators is expected to decrease with increasing speed due to the expected change in modal strain distributions with centrifugal loading.,[8] for example, demonstrated this latter effect on a two-bladed rotor case.

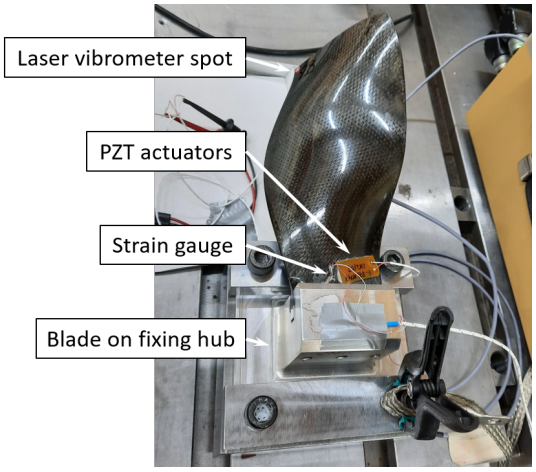

FIGURE 6. Single blade testing set-up for piezoelectric excitation system assessment at rest on the fixing hub

Setup for individual blades' characterization. Each blade is clamped on a suspended fixing hub (Figure 6). It is equipped with a strain gauge and two piezoelectric actuators. Screws net force is equivalent to the centrifugal force expected at 100% Nn (11000 rpm). Tightening torque is controlled by a torque-meter $2-10$ Nm. In spite of its simplicity, this static load application device has revealed significantly repeatable, qualifying it for relevant mistuning quantification. Of course, each measurement in Figure 6 needs blade's mounting / dismounting process. Also, these measurements agree with those presented in.[2] Blade's frequency sensitivity to temperature is also quantified at this step and estimated to $-0.1\%/°C$.

The experimental set-up also includes a laser vibrometer and a PZT actuators amplifier, with single channel signal generator and digital signal processing unit.

FRFs are measured with the strain gauge and a laser vibrometer pointing at the blade's tip leading edge along the Y axis, as defined in Figure 3. Stepped sine frequency excitation is used[9] with constant voltage amplitude through 1F and 2F resonances. Note that strain level is useful for comparison with aerodynamic experiments whereas laser vibrometer measurement will be more convenient for comparison with FEM results. Temporal periods number for each frequency step is adjusted to ensure that response's transient part has become negligible in front of the steady state part. So FRFs are computed at a number of discrete frequencies.

Preliminary impact hammer tests. Impact hammer preliminary modal tests are performed on blades before and after piezoelectric actuators are glued. In both cases the rest of the set-up is the same. Frequencies are identified using a classical SDOF peak-picking identification technique applied to isolated resonances. Figures 7a and 7b show blade frequency distributions obtained for the two first bending modes.

The first observation is that piezoelectric material addition shifts frequencies upwards and, therefore, has a stiffening effect which is consistent with the fact that they are implemented close to clamped boundary conditions. The mean frequency (dotted lines on Figure 7) for the first bending mode increases from 243.9 Hz to 245.4 Hz ($+0.6\%$). For the second bending mode, the frequency moves from 591.0 Hz to 593.9 Hz which corresponds to an increase of $+0.5\%$. Frequencies relative dispersion (σ/Σ, ie standard deviation divided by mean value) is 0.4%. This value quantifies the so-called tuned blade set. This perturbation may seem of the same order of blade's set natural dispersion but more important is the fact that this perturbation acts as a global shift for all blades, therefore preserving the pattern of the frequency distribution for the two modes. This may be considered as satisfactory since, once again, the aim is to preserve as much as possible all experimental conditions between aerodynamic and vacuum experiments.

Actuators efficiency assessment. Piezoelectric actuators efficiency is evaluated from the amplitudes reached, which are summarised together with modal properties on Table 1. First bending mode mean strain amplitude

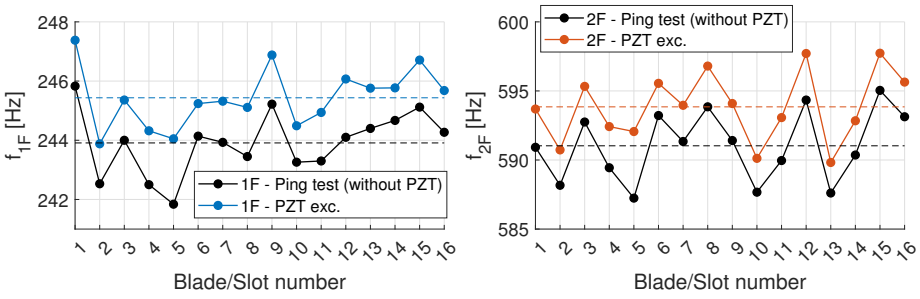

(a) (b)

FIGURE 7. Comparison between individual blade eigenfrequency before and after piezoelectric actuators installation. a) 1F, b) 2F.

Mode	**1F**	**2F**
$\|Z\|$ $[\mu m]$	162 (5.9%)	295 (6.1%)
$\|\varepsilon\|$ $[\mu def]$	90 (11%)	47 (9.1%)
f $[Hz]$	245.5 (0.4%)	593.9 (0.4%)
ξ $[\%]$	0.33 (3.0%)	0.30 (3.9%)

TABLE 1. Single blade validation results for the 16 blades of tuned configuration with actuators. Mean value (Relative dispersion).

at resonance corresponds to $90\mu def$ which correspond to 20% of the scope limit and $47\mu def$ (18% of the scope limit) for the second bending mode. Assuming, at this step, that single blade tests are representative of rotating tests (to be demonstrated at next step), obtained amplitudes are promising since NSV and SV responses in,[2] a part of the objectives is achieved. Moreover the blade's set has proven to be quite homogeneous in term of properties and response amplitudes. Even if Table 1 raw results seem fair in terms of dispersion, it should be noted that actuators excitation homogeneity is blurred by the fact that individual blades damping ratios vary, with direct influence on the amplitude at resonance. Interestingly, but not detailed here, results compensated from deviations of individuals damping ratios are even better assessing the homogeneity of actuators along the blade set.

Numerical vs experimental single blade comparison. Initial numerical results, before updating, are shown on Table 2's first line, with $\xi = 0.2\%$ as typical damping value for structural dynamics calculation. The numerical model has been updated by adding a polyimide layer (Young's modulus : $E = 5\ Gpa$, density : $1.5\ g/cm^3$) of $0.2\ mm$, to be more representative of actual actuator encapsulation. Amplitudes are divided by 1.4 with the polymer layer, which is physically interpreted by piezoelectric actuator transmitted force attenuation, due to polyimide layer interface. Then, modal damping ratios have been also updated from 0.2% to 0.33% for the first bending mode and 0.30% for the second bending mode. Numerical results are summarized on Table 2 and relative errors with experimental values are given in parentheses.

Numerical results are compared with the 16 blades experimental mean values (amplitudes, frequencies). The good correlation obtained allows us to conclude that numerical model and results are quite predictable and can be used with confidence when predicting rotating fan dynamics (not detailed here).

Mode	**1F**	**2F**
$\|Z\|$ $[\mu m]$, $\xi = 0.2\%$	358	657
$\|Z\|$ $[\mu m]$, ξ updated	154 (-4.9%)	312 ($+5.8\%$)
f $[Hz]$	248.7 ($+1.4\%$)	593.8 (-0.02%)

TABLE 2. Single blade numerical predicted amplitudes before model update (1F, 2F) with $\xi = 0.2\%$ (first row). Numerical predictions with ξ adjusted from 0.2% to mean actual experimental values. Numerical value (relative error with the experimental value).

2. EXPERIMENTAL MEANS AND METHODS

2.1 Vacuum test rig conditions

Figure 1 overall view shows the complete test rig used for the experiments. The composite fan assembly is mounted by a bolted flange to Phare-1 high speed shaft. The latter has recently been upgraded by a gearbox integration to allow bladed discs to be driven at higher speeds by the electric motor. For these experiments, the gear ratio used is 3.125, while drive variator has been parametrised to limit shaft speed to 12000 rpm. Speed variation during FRF measurements is less than 0.1%.

A vacuum chamber dedicated to the sub-scale fan was designed and used instead of the original one used for the full-scale rotors.[10] The multi-way slip-ring unit connected to the shaft allows electrical power to be transferred from the stationary frame to the rotating piezoelectric elements. A telemetry electronic box, for strain gauge conditioning and signal transmission to stationary frame, is supported by the shaft. Residual rotating-seal air leakage is entered and exhausted at the rear of the fan. Chamber's limit pressure, of 0.1 $mbar$, and temperature are monitored by a pressure sensor and a Pt100 temperature sensor. Temperature variation inside the chamber is between $20°C$ and $27°C$ for the whole test campaign, depending mainly on the tested speed. Variation during a particular measurement is negligible.

The vacuum chamber also acts as a containment shield. Radial tip clearance between vacuum chamber's inner surface and blades' tips is one or two orders of magnitude larger (1 cm) than usual values in air, as it can be distinguished in Figure 2, preventing any influence on blade's dynamics. Under these conditions, with piezoelectric excitation switched off, no signature was detected on the rotating blade signals, confirming the vibratory environment quality. Rig's various components vibration levels are monitored by means of accelerometers for all stationary parts and non-contact probes for rotating shafts. Embedded piezoelectric patches are driven by a 16-channels power amplifier via the slip-ring and wires passing through rig's hollow shafts, up to the fan.

2.2 Travelling waves stepped sine tests

Rotating fan's modal testing is performed using a multichannel stepped sine excitation signal to drive piezoelectric actuators, which produce travelling wave excitations with specific ND number (N_v). The sine signal is chosen in order to obtain the best possible signal to noise ratio and to easily exhibit potential non-linear effects. FRFs at constant voltage are estimated at steady states and will be treated by frequency modal identification methods. Inter-blade phase angles are adjusted to obtain forward or backward travelling wave excitation signal, according to Equation 1 :

$$U_k(t) = U_f \times \sin(\omega_{exc} t + \phi_k) + U_b \times \sin(\omega_{exc} t - \phi_k),\ k = 1, ..., N, \tag{1}$$

where, N is the number of blades, k is the index of a channel associated with a blade, N_v is the nodal diameter from 0 to $floor(N/2)$,$\phi_k = k2\pi\frac{N_v}{N}$ is the inter-blade phase angle, f_{exc} is the forcing frequency of the travelling wave signal $[Hz]$ related to $\omega_{exc} = 2\pi f_{exc}$ (the TW excitation pulsation).

The excitation frequency f_{exc} is stepped from f_{start} to f_{end} by increments of δ_f. At each step, the frequency is constant for a number of periods n, which must be carefully chosen to correctly approach steady state and avoid avoid FRF distortion.

Tests presented below use either a forward or a backward travelling wave, ie $U_f = 0$ or $U_b = 0$. These directions are relative to the rotation direction shown in Figure 2. Equation 1 follows the numbering convention in Figure 2.

All blades are simultaneously activated by the travelling wave signal, which drives each pair of their respective actuators with the adapted inter-blade phase angle. The measured responses are referenced to the signal $U_1(t)$, which is chosen as a reference for computing FRFs estimations ($[\mu m/m/V]$).

2.3 Modal extraction method

A modal curve fitting method is used to estimate modal frequencies, damping ratios and mode shapes from the measured FRFs that will be denoted $H(i\omega)$. The method uses a frequency domain response function model which is fundamentally based on the assumption of a linear, time-invariant system and expressed by Equation 2 :

$$\hat{H}(i\omega) = \sum_{l=1}^{n_p} \frac{R_l}{i\omega - \lambda_l} + \frac{R_l^*}{i\omega - \lambda_l^*} + R_\infty. \tag{2}$$

$\hat{H}(i\omega)$ is the FRF model vector, at pulsation ω, of size $N \times 1$ (with N the number of measured blades), expressed as a linear superposition of a number n_p of modal participations characterised by their respective residual vectors R_l and poles λ_l. R_l will be interpreted as mode shapes. i verifies $i^2 = -1$. Asterisks (*) stand for conjugate quantities. Additional term R_∞ takes into account the contribution of modes outside the measured frequency range. As the frequency ranges of interest are relatively narrow for the present application, the usual term which would have been $R_{-\infty}/\omega^2$ is omitted here. It should be emphasised that preliminary linearity tests were carried out by measuring the response to different levels of excitation to ensure the applicability of the linear model. Maintaining stationary test conditions, such as speed, temperature, and pressure, allows for the hypothesis of an invariant system. Repeatability checks were conducted throughout the test campaign to ensure that the system's response to a reference excitation remains consistent.

The poles will be related to natural angular frequencies ω_l and damping ratios ξ_l using Equation 3 :

$$\begin{aligned} \omega_l &= |\lambda_l| \\ \xi_l &= \frac{-Re(\lambda_l)}{\omega_l} \\ \lambda_l &= -\xi_l\omega_l + i\omega_l\sqrt{1-\xi_l^2} \end{aligned} \tag{3}$$

where ξ_l and ω_l are the viscous damping ratio and the natural angular frequencies of the $l-th$ mode respectively. The so-called natural frequencies would be $f_l = \omega_l/2\pi$.

The identification process aims to solve for the unknown modal parameters R_l, λ_l for $l = 1...n_p$ and R_∞ by minimising a fit error function between the measured data and the corresponding response model $\hat{H}$ for each blade and for all discrete measured frequencies obtained from the stepped sine test.

Note that the number n_p, which determine the order of the pole identification problem, is unknown a priori and must be treated as explained below.

The two main steps of the applied Least Square Rational Function (LSRF) method are the determination of the poles in a first sophisticated non-linear least square minimization process in the frequency domain and then the resolution for the residual vectors R_l and R_∞ using a linear least square problem. The linear least square problem conditioning has been improved from an available implementation by suppressing conjugate terms of Equation 2 which are non-resonant and decaying for $\omega > 0$, leading to the linear problem expressed by Equation 4 :

$$\begin{bmatrix} H(i\omega_{start}) \\ \vdots \\ H(i\omega_{end}) \end{bmatrix} \underset{LS}{=} \begin{bmatrix} \frac{1}{i\omega_{start}-\lambda_1} & \cdots & \frac{1}{i\omega_{start}-\lambda_{np}} & 1 \\ \vdots & \cdots & \vdots & \vdots \\ \frac{1}{i\omega_{end}-\lambda_1} & \cdots & \frac{1}{i\omega_{end}-\lambda_{np}} & 1 \end{bmatrix} \begin{bmatrix} R_1 \\ \vdots \\ R_{n_p} \\ R_\infty \end{bmatrix} \tag{4}$$

The whole procedure is described in detail in,[10,11] together with the definition of the fit error Frobenius norm and more. The method could be qualified as global in the sense that the poles are common to all simultaneously measured FRFs on all blades, thanks to strain gages and the telemetry system.

To determine a best order parameter n_p, we choose a heuristic iterative method on that parameter as follows. The poles and residuals identification is performed by applying the LSRF method first with $n_p = 1$ and then with successive incremental orders until the fit error and the modal parameters values become practically stationary as n_p increases. This will be illustrated in application below, by frequency stabilization plots showing successively identified frequencies and corresponding fit error function values over n_p that will help to choose the value for parameter n_p in each case.

3. EXPERIMENTAL ROTATING RESULTS AT VACUUM

Two types of experiments are discussed in this section. The first one uses a forward travelling wave with six nodal diameters exciting 1F modes and is denoted 1F+6ND. Secondly, modal tests on 2F modes are presented using a backward travelling wave with four nodal diameters and labelled 2F-4ND. Respectively, these can be related to an analysis of NSV at 9766 rpm showing a 6ND forward travelling structural response of 1F modes at 266.2 Hz with a mean level of 40 $\mu m/m$ over rotor strain-gauges and a four nodal diameters backward SV at the 2F-4EO crossing on the Campbell diagram at 10000 rpm (90 $\%Nn$) showing a response at 660.66 Hz with a level of 8 % of the scope limit equivalent to 20 $\mu m/m$.[2] Note that with Phare-2, NSV tests are performed at constant speed, whereas synchronous vibration is obtained with a slow acceleration at a constant ramp of 25 rpm/s. All modal tests are performed at constant speed as in Phare-1. The possible effect of acceleration is not discussed in this paper.

3.1 Modal analysis of measured FRFs

Figure 8 presents the modulus of measured FRFs, curve fits and modal participations for the modal test 1F+6ND performed at the actual speed $\Omega = 88\%\ Nn$ (9680 rpm) and with $U_f = 200\ V$. It is noticeable that several frequencies are responding with significant variations of amplitudes over the 16 blades. The curve fit matches accurately the measurements with a reduced number of poles explaining resonant peaks on frequency response functions. In this case, 7 poles are identified which are localised by grey vertical lines on the frequency axis of the 16 diagrams. The modal participation of the globally dominant mode n°5 is plotted in orange and the second one in yellow. Unfortunately, the signal of strain gauge associated to the slot 1 was lost during the experimental campaign. One can notice that modal participations are not equally distributed in amplitude over the blades as if would have been the case for a ideal tuned case. Although, the RMS amplitude of modal participations for mode n°5 computed over the 16 blades is on the order of 40 $\mu m/m$ which demonstrates the representativeness of obtained dynamic levels. To go further, an analysis of the residual vector R_5 is proposed in Figure 11 (up) where its components are plotted against blade numbers. The plot shows a complex mode shape which modulus, real and imaginary parts are detailed. As expected, this mode doesn't have a simple shape with a clearly determined number of ND and has prominent components at blades n°3, 8, 13. The modulus of the discrete spatial Fourier transform is plotted in Figure 11 (bottom). Interestingly, is the detection of the major component at index $N_\nu = +6$, which corresponds to the ND number of the wave excitation. However, there are some other significant components (see $N_\nu = -7$). It should also be noted that in the absence of the gauge at blade n°1, an equal amount of energy is distributed among all the components $N_\nu = -8$ to $+7$, but it is believed that is doesn't change this status. Other modes, such as the one at 274.12 Hz, have similar characteristics (not detailed here).

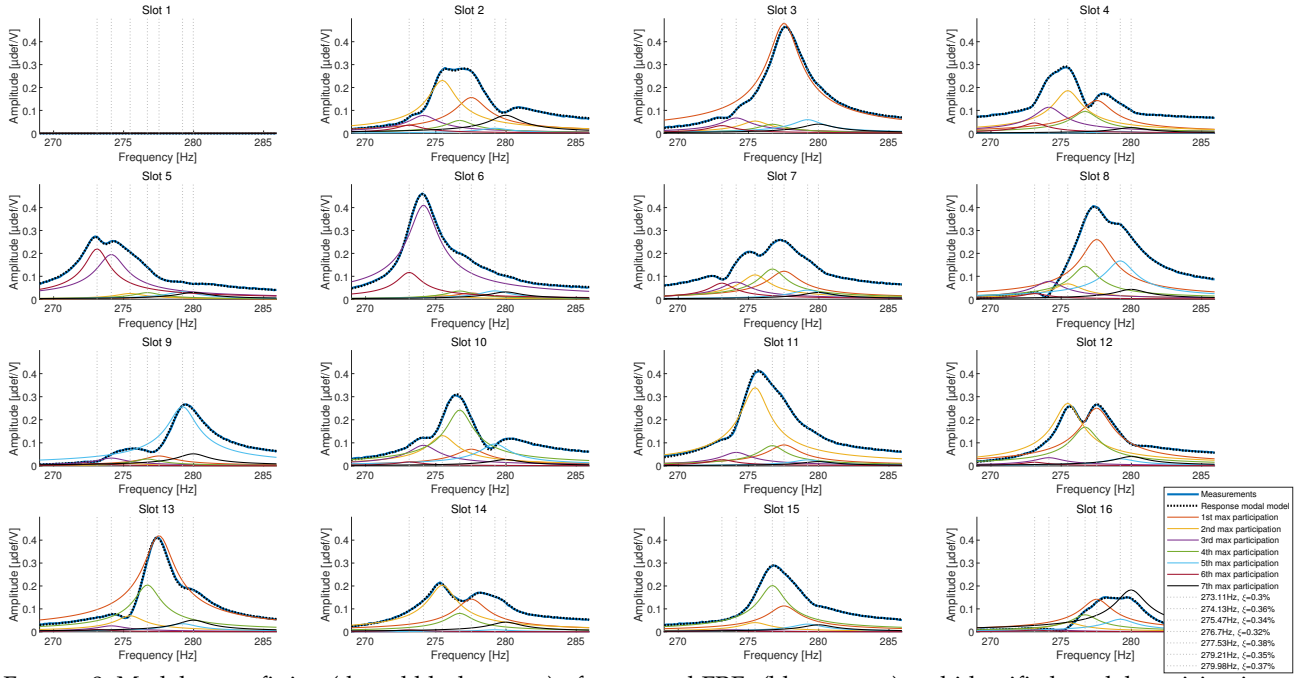

FIGURE 8. Modal curve fitting (dotted black curves) of measured FRFs (blue curves) and identified modal participations - Modal test 1F+6ND (88% Nn, $U_f = 200\ V$). The slot numbers correspond to disk position of blades. ref : 20231115 – 120741 e3

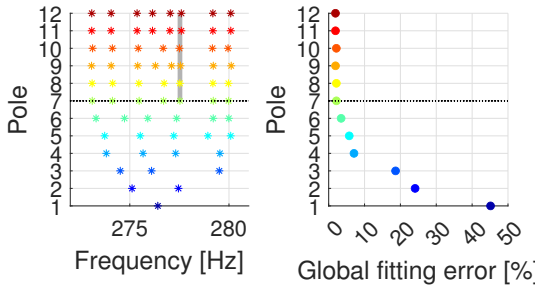

FIGURE 9. A modal test 1F+6ND (88% Nn, 200 V). a) Stabilization diagram, b) Global fitting error. In grey, stabilization chimney of mode 5.

Referring to,[12] the localised nature of a mode shapes can be related to the frequency versus ND plot shown in Figure 10 where horizontal lines corresponds to modes with a low structural coupling between blades. On the contrary, so called disc dominant modes with higher structural coupling are limited to only very first low ND indexes for which the line is "slented" in the plot. As shown in the literature, the degree of mode localization depends on the mistuning-to-coupling ratio. therefore, as NDs increases, the modes will have low inter-blade coupling and therefore localised modes revealed also by a multiple harmonic content as in Figure 11. The modal shapes aspect is in accordance with the frequency versus ND.

In the previous case (modal test 1F+6ND, 88% Nn, 200 V, Figure 8), 7 poles has been selected, the choice of the number of poles is based on 2 criteria, the global fitting error and the stabilization digram illustrated on Figures 9. Poles are stable in frequency, the grey chimney of mode 5 on the graph is stable with a frequency variation of $\pm 0.04\%$ and the global fitting error stabilizes and is less than 2%.

3.2 Parameters influence

The influence of velocity on frequencies are generally well predicted by the finite element method. However, it is necessary to assess the degree of frequency correlation between model and real systems for consistency and

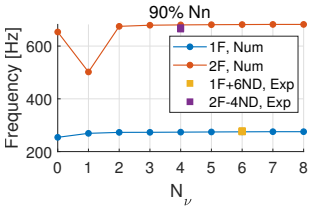

FIGURE 10. Numerical frequency vs nodal diameter diagram, squares represent experimental values from 1F+6ND and 2F-4ND modal tests.

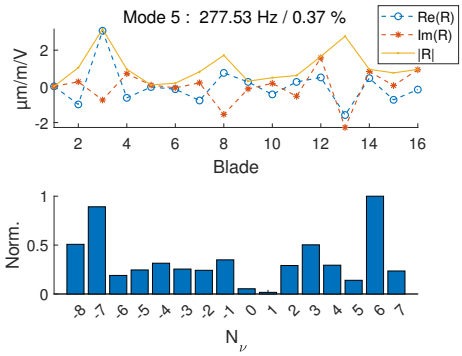

FIGURE 11. Residual vector R_5 - the dominant mode in 1F+6ND modal test. Up : space representation, real, imaginary parts and modulus $Re(R_5)$, $Im(R_5)$, $|(R_5)|$. Bottom : spatial Fourier spectrum of R_5.

confidence purposes. On the other hand, the prediction of damping and possible associated non-linear effects requires considerable effort and can hardly be done without experimental validation at the end.[6] Furthermore, in case of frictional damping it can be sensitive to speed due to the centrifugal load. Since instability generally occurs at a certain critical speed, it may be crucial to establish the damping-speed relationship for predicting its occurrence. Modal analysis under vacuum will provide damping ratios that can be used in the structural part of FE models for accurate predictions.

Table 3 presents the evolution of the frequency and the modal damping ratio according to the piezoelectric voltage for the modal tests 1F+6ND and 2F-4ND. A slight non-linear effect was put in evidence by the shift of frequencies as the piezoelectric voltage and therefore amplitude increased. Thanks to the accuracy of the modal tests performed, even small these frequency shifts are significant and physically consistent with frictional damping, as they are known to decrease with amplitude in that case. However, the expected associated decrease of damping ratio couldn't be distinguished from the data due to higher uncertainties on this parameter. The damping ratio can be considered constant namely 0.4% (resp. 0.3%) for the first (resp. second) bending mode. Technically, the friction probably occurs in dovetail joints of blades and is very limited in this case due to the centrifugal load. Interestingly however, this demonstrate that from a structural point of view, the behaviour during the NSV analysis can be considered as linear in that case.

Figure 12 shows the evolution of the frequency response (slot 3) as a function of speed and piezoelectric voltage for the first bending mode tests (1F+6ND). The maximum rotor speed is 11000 rpm. At constant voltage the modal frequency increases with the centrifugal load. The black dot represents the NSV Phare-2 result at the

U_f or U_b	**1F+6ND**	**2F-4ND**
40 V	278.3 Hz (0.43%)	667.1 Hz (0.32%)
120 V	277.9 Hz (0.38%)	666.8 Hz (0.32%)
200 V	277.5 Hz (0.38%)	666.3 Hz (0.30%)

TABLE 3. Evolution of the modal frequency and the damping ratio according to the piezoelectric voltage for the modal tests 1F+6ND and 2F-4ND.

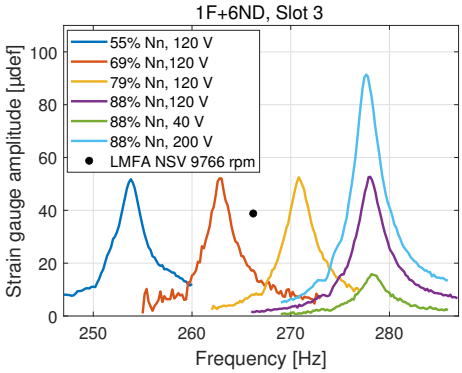

FIGURE 12. Amplitudes of the frequency responses (Slot 3) for the dominant mode in modal test 1F+6ND at rotational speeds 55, 69, 79 and 88% Nn and piezoelectric voltages (40, 120, 200 V).

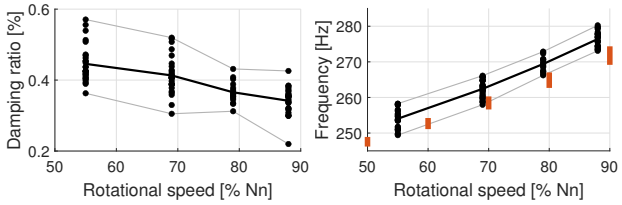

(a) (b)

FIGURE 13. Evolution of the modal damping ratio (a) and the frequency (b) according to the rotational speed for the modal tests 1F+6ND. Red bars : FEM frequencies for $N_\nu = 1$ to 8.

rotor speed of 9766 rpm, a relative difference of 4.4% is observed on the frequency.

The evolution of modal damping ratios and frequencies according to the rotational speed from modal tests 1F+6ND is presented on the Figure 13. For each rotational speed, the mean, the minimal and the maximal values are computed. An average trend (black line) and an envelope (min,max) (gray lines) are plotted. This plots combine all selected modal parameters from a series of 17 different modal tests, including voltage and speed variations and repeatability checks. Modes 1F with dominant 0ND and 1ND component are outside the measurement frequency range.

Over all the test series of this mode, the damping ratios decrease with the speed. FEM predictions in rotation made it possible to highlight that the efficiency of the piezoelectric actuator drops as a function of the regime due to the modification of the modal shape for a constant damping ratio in the calculation.[8] Therefore, Figure 12 shows that this damping ratio reduction compensates the amplitude reduction implied by the increase of the rotational speed.

The mean value of the damping ratio moves from 0.45% at 55% Nn to 0.34% at 88% Nn, this represents a decrease of 24%. The mean frequency moves from 254.0 Hz at 55% Nn to 276.4 Hz at 88% Nn, which corresponds to an increase of 9%.

Figure 14 shows the evolution of the frequency response (slot 6) depending on the rotational speed and the piezoelectric voltage for the second bending mode tests (2F-4ND). The same analysis can be carried out for the test series of second bending mode which is composed of 10 different modal tests (voltage, speed variations and repeatability checks) and the mean value of the modal damping ratio moves from 0.35% at 55% Nn to 0.31% at 88% Nn, this represents a decrease of 11%. The mean frequency moves from 621.0 Hz at 55% Nn to 667.0 Hz at 88% Nn, which corresponds to an increase of 7% (Figure 15). The black dot represents the NSV Phare-2 result at the rotor speed of 10000 rpm, a relative difference of 0.9% is observed on the frequency.

FEM prediction of blade eigenfrequencies are represented in red on the Figures 13 and 15 for $N_\nu = 1...8$ for the mode family 1F and from $N_\nu = 2...8$ for the modes 2F.

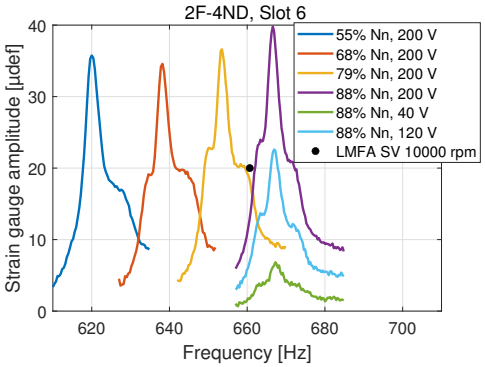

FIGURE 14. Amplitudes of the frequency responses (Slot 6) for the dominant mode in test 2F-4ND at rotational speeds 55, 68, 79 and 88% Nn) and piezoelectric voltage (40, 120, 200 V).

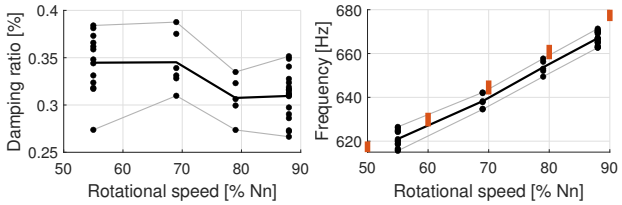

(a) (b)

FIGURE 15. Evolution of the modal damping ratio (a) and the frequency (b) according to the rotational speed for the modal tests 2F-4ND. Red bars : FEM frequencies for $N_\nu = 2$ to 8.

Conclusions and perspectives

The ECL5 composite-material fan stage, representative of near future UHBR architecture, has been investigated under vacuum conditions in order to characterize its structural behaviour, mainly the structural damping of the whole fan blade assembly. The originality of the approach lies in the fact that a same composite fan specimen has been tested in aerodynamic conditions and then at vacuum at equivalent conditions in term of speed and vibration state.

The instrumented fan blades have been firstly tested individually on a suspended fixing hub at rest. The optimal position of the piezoelectric actuators has been chosen thanks to a electromechanical finite element model. Frequencies dispersion of individual blades is quantified and shows in particular that the added exciters have negligible influence on the dynamics, especially on mistuning. Experimentally, piezoelectric actuators efficiency, implemented under inter blades platforms, is demonstrated by reaching representative amplitudes.

Once the fan has been installed in the Phare-1 test rig, the vibration patterns have been reproduced through travelling waves piezoelectric excitation. Measurements and experimental modal analyses data are consistent with the calculation and aerodynamic measurements performed in the Phare-2 test rig particularly in terms of amplitudes.

At maximum excitation, slight structural non-linear effect is observed on identified modal parameters. But can be neglected on the range of NSV response amplitudes tested, and for the tested rotating speeds. This provides a justification for the assumption of a linear structural model which could useful in multi-physics numerical simulations. The numerical model gives a satisfactory assessment of vacuum tests in terms of frequency. It has been observed that the 1F modes of the tuned fan configuration are localized due to the low structural coupling between blades.

Modal damping ratio has been identified for twos sets of several modes within the 1F and 2F families which are mainly sensitive to the rotational speed. Globally, modal damping ratios decrease by 24% (resp. 11%) in relation to rotational speed for the first bending mode family 1F (resp. 2F). Thanks to the large amount of accurate data collected, measured structural damping ratios can be introduced into model for numerical simulations of aeroelasticity.

Acknowledgements

The results presented in this paper rely on the contributions of a large research group. The authors particularly thank Cedric Desbois, Benoit Paoletti, Anne-Lise Fiquet, Alexandra P. Schneider, Xavier Ottavy, Christoph Brandstetter of LMFA, Stephane Lemahieu, Abdelhakim Ezzerouki, Sebastien Leone of ECL, for their support and contributions to the experiments.

The presented research was supported through Clean Sky 2 Joint Undertaking (JU), CATANA project, under grant agreement N°864719. The JU receives support from the European Union's Horizon 2020 research and innovation programme and the Clean Sky 2 JU for members other than of the Union. This publication reflects only the author's view and the JU is not responsible for any use that may be made of the information it contains.

Functioning of the test facility was enabled through financial supports of Agence Nationale de la Recherche (ANR, EquipEx Project PHARE). Buildings and infrastructure were supported by ECL, telemetry electronics partly supported by Institut Carnot (INGENIERIE@LYON - MERIT Project).

REFERENCES

[1] V. Pagès, P. Duquesne, S. Aubert, L. Blanc, P. Ferrand, X. Ottavy, and C. Brandstetter, "Uhbr open-test-case fan ecl5/catana," *International Journal of Turbomachinery, Propulsion and Power* **7**(2), p. 17, 2022.

[2] A.-L. Fiquet, A. P. Schneider, B. Paoletti, X. Ottavy, and C. Brandstetter, "Experiments on tuned uhbr open-test case fan ecl5/catana : stability limit," 2023.

[3] N. Ombret, R. Daon, A. Dugeai, F. Thouverez, and L. Blanc, "A frequency-time partitioned approach for computing fan blade flutter induced limit cycle oscillations with nonlinear friction on contact interfaces," in *Turbo Expo*, **87059**, p. V11AT21A010, ASME, 2023.

[4] S. Rodríguez-Blanco, J. González-Monge, and C. Martel, "Interaction of flutter and forced response in a low pressure turbine rotor with friction damping and mistuning effects," *Journal of Sound and Vibration* , p. 118181, 2023.

[5] M. Lassalle and C. Firrone, "A parametric study of limit cycle oscillation of a bladed disk caused by flutter and friction at the blade root joints," *Journal of Fluids and Structures* **76**, pp. 349–366, 2018.

[6] A. Mabilia, C. Gibert, F. Thouverez, and E. De Jaeghere, "Nonlinear forced response of a composite fan blade actuated by piezoelectric patches : Simulation and testing," in *Nonlinear Dynamics, Volume 1 : Proceedings of the 36th IMAC, A Conference and Exposition on Structural Dynamics 2018*, pp. 351–362, Springer, 2019.

[7] C. Brandstetter, V. Pages, P. Duquesne, B. Paoletti, S. Aubert, and X. Ottavy, "Project phare-2—a high-speed uhbr fan test facility for a new open-test case," *Journal of Turbomachinery* **141**(10), p. 101004, 2019.

[8] J. B. Min, K. P. Duffy, B. B. Choi, A. J. Provenza, and N. Kray, "Numerical modeling methodology and experimental study for piezoelectric vibration damping control of rotating composite fan blades," *Computers & Structures* **128**, pp. 230–242, 2013.

[9] M. Friswell and J. Penny, "Stepped sine testing using recursive estimation," *Mechanical Systems and Signal Processing* **7**(6), pp. 477–491, 1993.

[10] C. Jorajuria, C. Gibert, F. Thouverez, and C. Esteves, "Experimental modal analysis of a full-scale rotating fan," in *Turbo Expo : Power for Land, Sea, and Air*, **86076**, p. V08BT27A021, American Society of Mechanical Engineers, 2022.

[11] A. A. Ozdemir and S. Gumussoy, "Transfer function estimation in system identification toolbox via vector fitting," *IFAC-PapersOnLine* **50**(1), pp. 6232–6237, 2017.

[12] M. P. Castanier and C. Pierre, "Modeling and analysis of mistuned bladed disk vibration : current status and emerging directions," *Journal of Propulsion and power* **22**(2), pp. 384–396, 2006.